Estimation of the spectral, electrical, and dielectric properties of Mn-Cu-Cd-Gd ferrite\graphene nanoplatelets composites

Z. Latif[a], A. U. Rehman[a], M. Yusuf[b], N. Amin[a], M. I. Arshad[a,*]
[a]*Dept. of Physics, Government College University, Faisalabad, 38000, Pakistan*
[b]*Department of Clinical Pharmacy, College of Pharmacy, Taif University, Taif 21944, Saudi Arabia*

The sol-gel auto combustion route was used to synthesis Mn-Cu-Cd-Gd ferrite\graphene nanoplatelets composites having chemical formula $Mn_{0.5}Cu_{0.25}Cd_{0.25}Fe_{1.97}Gd_{0.03}O_4$/Graphene nanoplatelets (MCCFG/GNPs composites) (where GNPs wt% = 0.0wt%, 1.25wt%, 2.5wt%, 3.75wt%, 5wt%). The incorporation of GNPs in the MCCFG sample enhanced the crystallite size from 35.89 nm to 58.92 nm. Raman modes of vibration also confirmed the spinel structure. The resistivity was reduced and optical bandgap energy was increased with increasing content of GNPs. Moreover, both dielectric constant and saturation magnetization was reduced with the insertion of GNPs in the MCCGF spinel lattice.

(Received May 16, 2022; Accepted August 16, 2022)

Keywords: sol-gel auto combustion; composites; crystallites size; dielectric; magnetization.

1. Introduction

Graphene attracted a lot of attention due to its applications in different fields including condensed matter physics, spintronics, material science, nanomedicine, tissue engineering, biology, and electronics [1]. The rapid electron mobility, high electrical conductivity, surface area with excellent mechanical strength, etc. are all characteristics of graphene. Graphene is a two-dimensional sheet made of sp^2 hybridized carbon and has the structure of a honeycomb. Due to its stability, low cost of manufacturing, and lightweight, graphene has also been explored among other electromagnetic materials. However, graphene's high dielectric qualities also lead to an agglomeration of graphene, poor impedance matching, and a low absorption property. Combining graphene with ferrites can overcome this problem. By employing ferrites in place of rare earth (RE) metal nanostructures, which serve as spacers between graphene nanosheets, the aggregation in graphene sheets was solved. The distortion in the structure and the modified properties of spinel ferrites (SFs) were reported by the introduction of different rare earth elements [2-4] and graphene content [5, 6]. Li *et al*., [7] reviewed the modifications in particle size and lattice parameters by the substitution of Nd ions and reduced graphene oxide (rGO) in Ni-Co-Zn ferrites. Zhao *et al*., [8] investigated the variation in particle size, morphology, distribution density, and microwave absorbance of Ni-Co-P composites with graphene nanosheets. Iftikhar *et al*., [9] reported the optical band gap of erbium-doped Ni-Co ferrite composites with rGO around 2.66 eV. Moreover, photocatalytic degradation was established for prepared nanocrystallites. Das *et al*., [10] prepared the composites of Co-Ni ferrites with reduced graphene successfully with the chemical reduction method. A decrease in particle size was stated with the addition of reduced graphene in prepared ferrites samples and the impact of reduced graphene on magnetic parameters was also discussed. Qamar *et al*., [1] investigated the composites of graphene with Ce doped nickel cobalt ferrites. An

* Corresponding author: mimranarshad@gcuf.edu.pk
https://doi.org/10.15251/JOR.2022.184.627

improvement in conductivity and magnetic properties was reported with the doping of graphene in Ce-Ni ferrites potentially making the prepared composites suitable for different electrical devices. Therefore, this work aims to investigate the impact of graphene nanoplatelets (GNPs) on spectral, optical and dielectric properties of $Mn_{0.5}Cu_{0.25}Cd_{0.25}Fe_{1.97}Gd_{0.03}O_4$/GNPs (GNPs wt% = 0.0wt%, 1.25wt%, 2.5wt%, 3.75wt%, 5wt%) composites (MCCFG/GNPs composites) prepared *via* the sol-gel auto combustion (SGAC) process.

2. Materials and methods

The MCCFG/GNP ferrite and their composites were synthesized by mixing all the nitrates including manganese, copper, cadmium, iron, gadolinium nitrates salts, and graphene nanoplatelets, and citric acid in the deionized water according to the stochiometric calculations. The mixed solution of all the nitrates, GNPs, and citric acid were put on the magnetic stirrer and by adding the solution of ammonia dropwise, the pH ~ 7 of the homogenous solution was maintained. The solution was heated at 80 ^oC and a gel was formed. After some time, the gel was changed into dry powder at 300 ^oC. This powder form of the sample was ground and put the sample into the muffle furnace at 800 ^oC for 8 hours of sintering. The step-by-step SGAC preparation of samples is represented in Fig. 1.

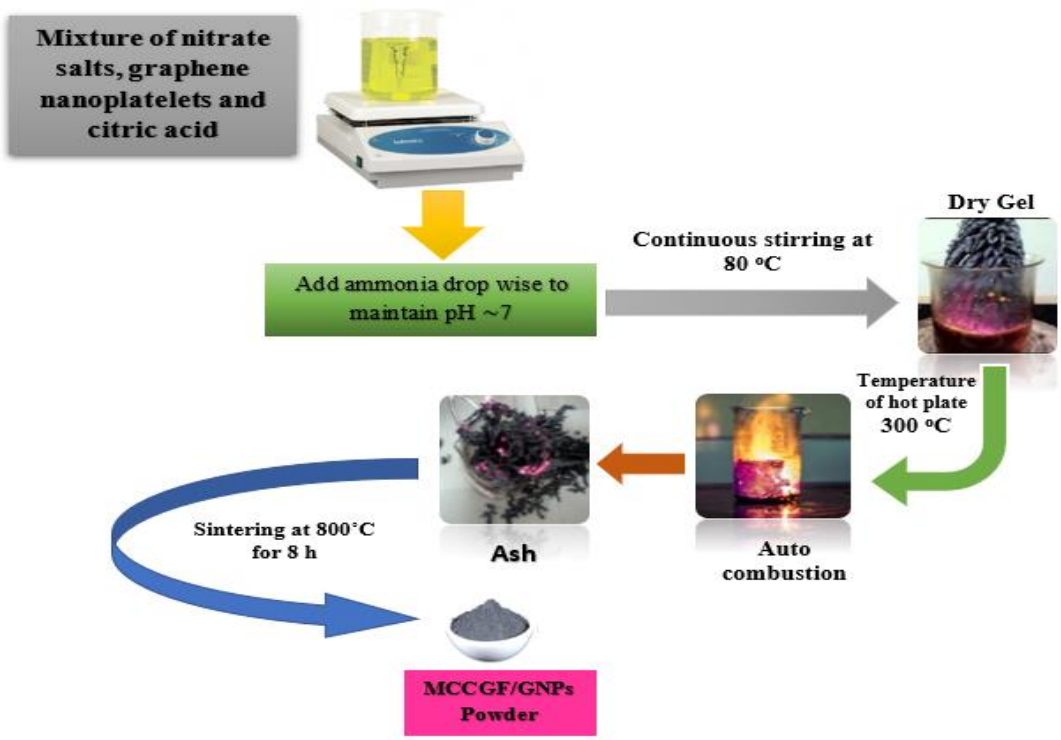

Fig. 1 Step-by-step SGAC of MCCFG/GNPs ferrite and their composites

2.1 Characterization techniques

Bruker D8 Advance, (Cu K_α source, λ = 1.54 Å) X-ray diffractometer (XRD) was used for structural analysis. The Raman and UV-visible spectroscopy were employed to find the vibrational modes and optical bandgap energy, respectively. LCR meter Model IM3536 was used to find the dielectric constant. Keithley Electrometer Model 2401 with two probes I–V measurement technique was used to find resistivity. The magnetic properties of samples were investigated at room temperature under an applied field ±5000 Oe.

3. Result and Discussion

3.1. X-Ray Diffraction Analysis

The XRD spectra of **MCCFG/GNPs** ferrite and their composites are shown in Fig. 2. The peaks at $2\theta = 30.24^{o}$, 35.35^{o}, 37.66^{o}, 43.57^{o}, 53.20^{o}, 56.13^{o} were observed corresponding to the planes (200), (311), (222), (400), (422), and (511) respectively. The crystallite size (*D*) was determined *via* Scherer's formula [11-13];

$$D = \frac{k\lambda}{\beta \cos\theta} \quad (1)$$

Where *k* is the constant shape factor and has a value of 0.94, and β represents the full width at half maxima (FWHM). The crystallite size was increased with the insertion of GNPs in the MCCFG sample (as shown in Table 1). It may be due to the incorporation of GNPs in ferrite lattice. The dislocation density (δ) was calculated with help of the formula given below [14];

$$\delta = 1/D^2 \quad (2)$$

The dislocation line density was reduced from 7.75×10^{-4} nm^{-2} to 2.87×10^{-4} nm^{-2}, as reported in Table 1. The interplanar distance (*d*) is to be determined by using the Braggs equation that is given below [15, 16];

$$2dsin\theta = n\lambda \quad (3)$$

where *n* is the order of reflection. The lattice constant (a) was estimated using equation [15, 16];

$$a = d\sqrt{h^2 + k^2 + l^2} \quad (4)$$

Here, *h k l* is the miller indices of the planes. The volume of the unit cell (*V*) was estimated *via* the below equation [16];

$$V_{cell} = a^3 \quad (5)$$

The lattice constant, interplanar distance, and unit cell volume were reduced with increasing the GNPs percentage and are given in Table 1. The increase in lattice parameters may be due to the incorporation of GNPs in the MCCFG lattice.

Table 1. Structural parameters of MCCFG/GNPs ferrite and their composites

Samples	2θ (degree)	h k l	D (nm)	$\delta \times 10^{-4}$ (nm^{-2})	d (Å)	a (Å)	V ($Å^3$)
MCCFG	35.35	311	35.89	7.75	2.5351	8.407	594.39
MCCFG/1.25wt%GNPs	35.35	311	35.89	7.75	2.5323	8.402	593.12
MCCFG/2.5wt%GNPs	35.4	311	57.90	2.98	2.5316	8.396	591.95
MCCFG/3.75wt%GNPs	35.41	311	58.09	2.96	2.5309	8.394	591.47
MCCFG/5wt%GNPs	35.42	311	58.92	2.87	2.5302	8.391	590.98

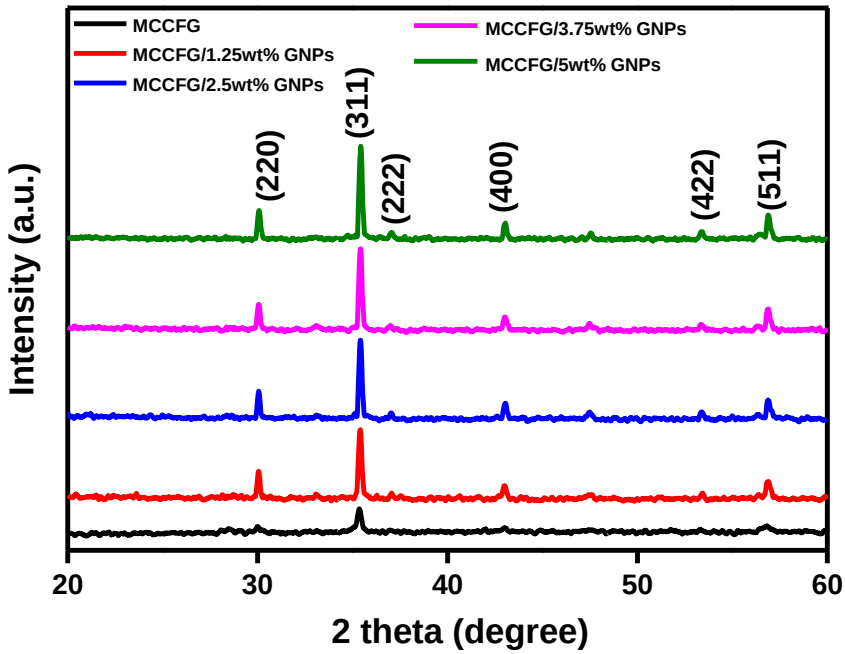

Fig. 2 XRD spectra of MCCFG/GNPs ferrite and their composites

3.2 Raman analysis

The **MCCFG/GNPs** ferrite and their composites Raman spectra in the range of 150 – 1000 cm^{-1} are shown in Fig. 3. The modes of vibration A_{1g}, E_g, $3T_{2g}$ are active Raman modes belong to spinel structure [17]. The A_{1g} mode shows the motion of O^{2-} anion and E_g and three T_{2g} correspond to the motion of both O^{2-} and cations. The values of $T_{2g}(1)$, E_g, $T_{2g}(2)$, $T_{2g}(3)$, and A_{1g} vibrational modes are reported in Table 2.

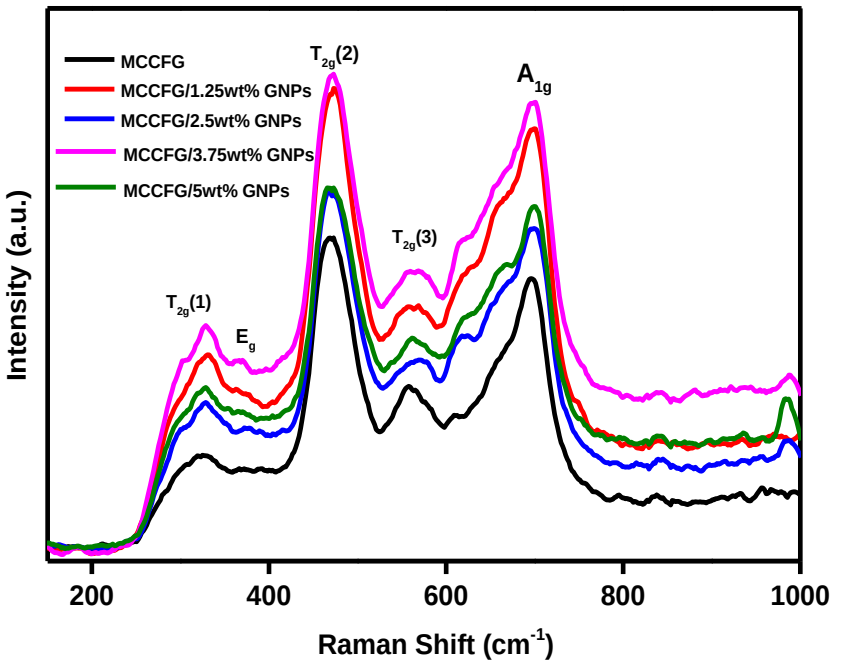

Fig. 3 Raman spectra of MCCFG/GNPs ferrite and their composites

Table 2. Raman modes of MCCFG/GNPs ferrite and their composites

Samples	T_{2g} (1)	E_g	T_{2g} (2)	T_{2g} (3)	A_{1g}
MCCFG	324	360	470	558	696
MCCFG/1.25wt%GNPs	326	362	465	572	698
MCCFG/2.5wt%GNPs	323	361	471	561	700
MCCFG/3.75wt%GNPs	331	358	469	563	697
MCCFG/5wt%GNPs	328	369	472	565	701

3.3 UV-vis analysis

MCCFG/GNPs ferrite and their composite's UV-visible spectra were recorded between 200–800 nm. The absorption coefficient (α) was estimated *via* the relation [18];

$$\alpha = 2.303 \log(A) / L \quad (6)$$

Here, A represents absorbance while t represents pallet thickness. The Tauc relation is given below [18];

$$\alpha h\nu = B (h\nu - Eg)^m \quad (7)$$

Here, B is a constant, hv is incoming photon energy, and m is constant. Fig. 4 showed the Tauc plots of as-prepared ferrite and their composites. It was noted from Fig. 5 that the optical bandgap energy (E_g) was increased *via* doping of GNPs in the MCCGF sample.

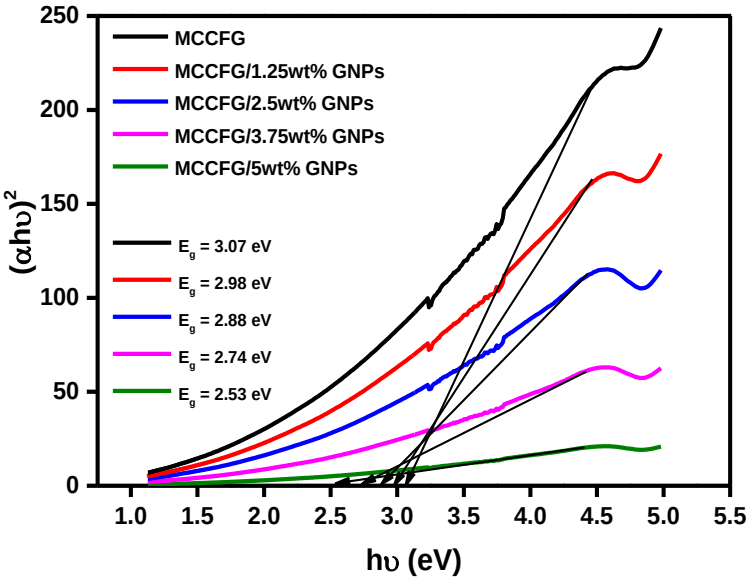

Fig. 4 Tauc plot

s of MCCFG/GNPs ferrite and their composites

3.4 Electrical analysis

The composition and synthesis method of the ferrite and their composites, which altered the cation distribution at the *A*- and *B*- sites, have an impact on resistivity. The following relation was used to determine resistivity [16];

$$\rho = RA/L \quad (8)$$

where *A*, *L*, and *R* indicate the area of pellets, the thickness of pellets, and resistance = 1/slope, respectively. The GNPs concentration % *versus* resistivity as depicted in Fig. 5. It was observed that the resistivity was decreased with the incorporation of GNPs in the MCCGF ferrite. The ferrites have high resistivity and GNPs have high conductivity. Therefore, the insertion of GNPs in the MCCGF sample reduced the resistivity.

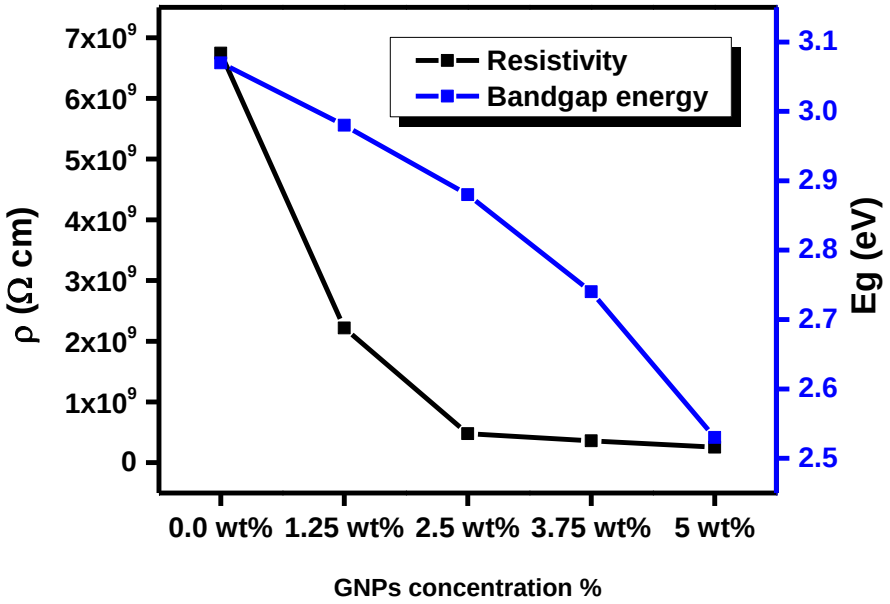

Fig. 5 GNPs concentration (%) versus resistivity of MCCFG/GNP ferrite and their composites

3.5 Dielectric analysis

The MCCFG/GNP ferrite and their composites dielectric constant *versus* frequency in Fig. 6. It was noted that the dielectric constant was reduced as frequency increased. The as-prepared ferrite and its composites exhibit no variation to the field at greater frequencies, which is explained by a slowing in electron hopping (EH) that reduced polarization. The EH at grain boundaries, which reduced the dielectric constant at high frequencies, was explained using the Koops and Maxwell-Wagner model [19]. Fig. 6 also showed that the incorporation of GNPs into the MCCFG ferrites reduced their dielectric constant.

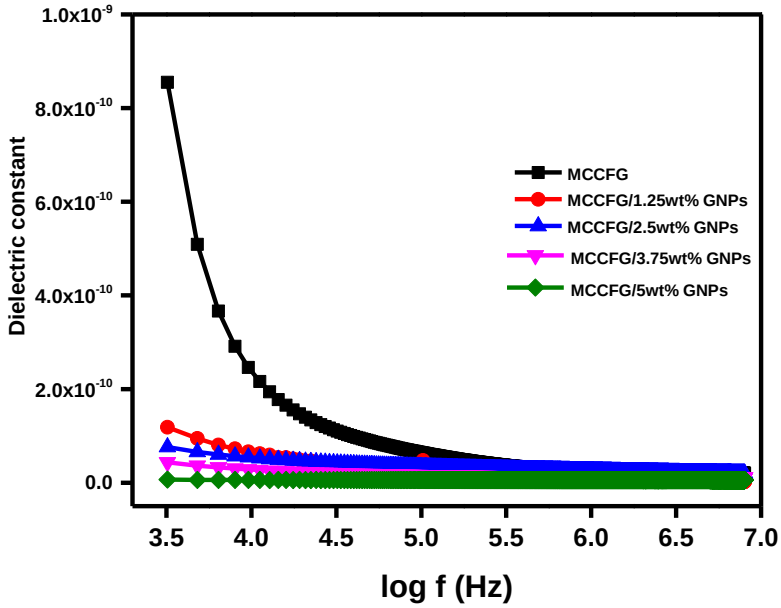

Fig. 6 Frequency versus dielectric constant of MCCFG/GNPs ferrite and their composites

3.6 Magnetic analysis

The hysteresis loops of MCCFG/GNPs ferrite and their composites are shown in Fig. 7 and magnetic parameters values are given in Table 3. The saturation magnetization (*M*s) was reduced from 118.93 to 89.53 emu/g with the substitution of GNPs in the MCCGF sample. The cations distribution plays a significant part in the variation of the ferromagnetic order of SFs [20]. The substitution of rare-earth elements introduces strong super exchange Heisenberg interactions in ferrites which are responsible for high magnetization. Moreover, in ferromagnetic structures, the interactions of the magnetic ions can be explained by Neel's sub-lattice theory [20, 21]. The remanence and coercivity were minimum for 5wt% concentration of GNPs. The squareness ratio (SQ = Mr/Ms) [22] for MCCFG/GNPs ferrite and their composites was also reduced with the addition of GNPs in the MCCFG sample. By the employment of the following relations of magneto crystalline anisotropic constant (*K*), and initial permeability (μ_i), were determined [18];

$$K = \frac{Hc \times Ms}{0.96} \tag{11}$$

$$\mu_i = \frac{M_S^2 \times D}{K} \tag{12}$$

It was observed that the minimum magneto crystalline anisotropic constant and maximum initial permeability were observed for GNPs 2.5wt% concentration.

Table 3. Magnetic parameters of MCCFG/GNPs ferrite and their composites

Samples	M_S (emu/g)	M_R (emu/g)	H_C (Oe)	SQ	K (erg/cm^3)	μ_i
MCCFG	118.93	60.21	728.99	0.506	90311.22	5.62
MCCFG/1.25wt%GNPs	112.36	47.36	352.82	0.421	41294.64	17.70
MCCFG/2.5wt%GNPs	106.61	48.51	375.54	0.455	41704.49	9.78
MCCFG/3.75wt%GNPs	94.81	45.35	317.64	0.478	31370.25	16.64
MCCFG/5wt%GNPs	89.53	24.70	154.77	0.275	14433.91	32.72

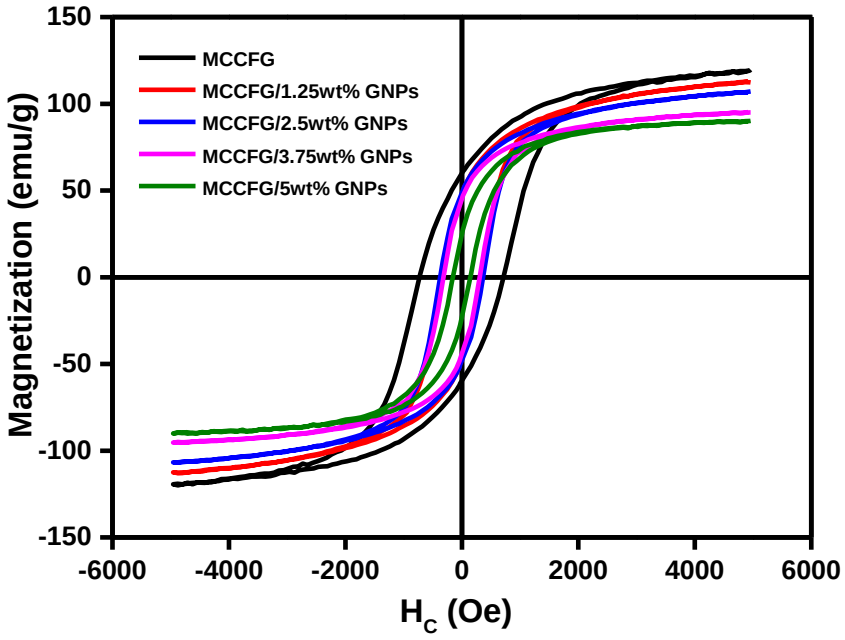

Fig. 7 M-H loops of MCCFG/GNPs ferrite and their composites

5. Conclusion

MCCFG/GNPs ferrite and their composites were prepared *via* the SGAC process and their structure was using XRD and Raman analysis. The lattice parameter including interplanar spacing, lattice constant and unit cell volume decreased with the incorporation of GNPs. The crystallite size and bandgaps energy were enhanced, while resistivity, dielectric constant, and magnetization were reduced with the additions of GNPs. Therefore, this material may be utilized for humidity sensors, antennas, micro memory chips, and catalytic activities.

Acknowledgements

Project supported by the Taif University Researchers Supporting Project number (TURSP-2020/293), Taif University, Taif, Saudi Arabia.

References

[1] S. Qamar, M.N. Akhtar, W. Aleem, Z. ur Rehman, A.H. Khan, A. Ahmad, K.M. Batoo, M. Aamir, Graphene anchored Ce doped spinel ferrites for practical and technological applications, Ceramics International, 46 (2020) 7081-7088.
https://doi.org/10.1016/j.ceramint.2019.11.200
[2] A.U. Rehman, N. Morley, N. Amin, M.I. Arshad, M.A. un Nabi, K. Mahmood, A. Ali, A. Aslam, A. Bibi, M.Z. Iqbal, Controllable synthesis of La3+ doped Zn0.5Co0.25Cu0.25Fe2− xLaxO4 (x = 0.0, 0.0125, 0.025, 0.0375, 0.05) nano-ferrites by sol-gel auto-combustion route, Ceramics International, 46 (2020) 29297-29308.
https://doi.org/10.1016/j.ceramint.2020.08.106
[3] A. Aslam, A.U. Rehman, N. Amin, M.A. un Nabi, Q. ul ain Abdullah, N. Morley, M.I. Arshad, H.T. Ali, M. Yusuf, Z. Latif, Lanthanum doped Zn0.5Co0.5LaxFe2− xO4 spinel ferrites synthesized via co-precipitation route to evaluate structural, vibrational, electrical, optical, dielectric, and thermoelectric properties, Journal of Physics and Chemistry of Solids, 154 (2021) 110080.
https://doi.org/10.1016/j.jpcs.2021.110080
[4] K. Hussain, N. Amin, M.I. Arshad, Evaluation of structural, optical, dielectric, electrical, and magnetic properties of Ce3+ doped Cu0.5Cd0.25Co0.25Fe2-xO4 spinel nano-ferrites, Ceramics International, 47 (2021) 3401-3410.
https://doi.org/10.1016/j.ceramint.2020.09.185
[5] S. Qamar, S. Yasin, N. Ramzan, A. Umer, M.N. Akhtar, Structural, morphological and magnetic characterization of synthesized Co-Ce doped Ni ferrite/Graphene/BNO12 nanocomposites for practical applications, Chinese Journal of Physics, 65 (2020) 82-92.
https://doi.org/10.1016/j.cjph.2020.02.023
[6] A.U. Rehman, F. Afzal, M.T. Ansar, A. Sajjad, M.A. Munir, Introduction and Applications of 2D Nanomaterials, 2D Functional Nanomaterials: Synthesis, Characterization and Applications, (2021) 369-382.
https://doi.org/10.1002/9783527823963.ch21
[7] J. Li, D. Zhou, W.-F. Liu, J.-Z. Su, M.-S. Fu, Novel and facile reduced graphene oxide anchored Ni-Co-Zn-Nd-ferrites composites for microwave absorption, Scripta Materialia, 171 (2019) 42-46.
https://doi.org/10.1016/j.scriptamat.2019.06.018
[8] S. Zhao, C. Wang, B. Zhong, Optimization of electromagnetic wave absorbing properties for Ni-Co-P/GNs by controlling the content ratio of Ni to Co, Journal of Magnetism and Magnetic Materials, 495 (2020) 165753.
https://doi.org/10.1016/j.jmmm.2019.165753
[9] A. Iftikhar, S. Yousaf, F.A.A. Ali, S. Haider, S.U.-D. Khan, I. Shakir, F. Iqbal, M.F. Warsi, Erbium-substituted Ni0.4Co0.6Fe2O4 ferrite nanoparticles and their hybrids with reduced graphene oxide as magnetically separable powder photocatalyst, Ceramics International, 46 (2020) 1203-1210.
https://doi.org/10.1016/j.ceramint.2019.08.176

[10] A. Das, P. Negi, S.K. Joshi, A. Kumar, Enhanced microwave absorption properties of Co and Ni co-doped iron (II, III)/reduced graphene oxide composites at X-band frequency, Journal of Materials Science: Materials in Electronics, 30 (2019) 19325-19334.
https://doi.org/10.1007/s10854-019-02293-x
[11] A. Aslam, A. Razzaq, S. Naz, N. Amin, M.I. Arshad, M. Nabi, A. Nawaz, K. Mahmood, A. Bibi, F. Iqbal, Impact of lanthanum-doping on the physical and electrical properties of cobalt ferrites, Journal of Superconductivity and Novel Magnetism, 34 (2021) 1855-1864.
https://doi.org/10.1007/s10948-021-05802-4
[12] N. Amin, M. Akhtar, M. Sabir, K. Mahmood, A. ALIa, G. Mustafa, M. Hasan, A. Bibi, M. Iqbal, F. Iqbal, SYNTHESIS, STRUCTURAL AND OPTICAL PROPERTIES OF Zn-SUBSTITUTED Co W-FERRITES BY COPRECIPITATION METHOD, Journal of Ovonic Research, 16 (2020) 11-19.
[13] I. ALIa, N. Amin, A. Rehman, M. Akhtar, M. Fatima, K. Mahmood, A. ALIa, G. Mustafa, M. Hasan, A. Bibi, ELECTRICAL AND MAGNETIC PROPERTIES OF BaCoxCd2-xFe16O27 W-TYPE HEXAFERRITES ($0\leq x\leq 0.5$), Digest Journal of Nanomaterials and Biostructures, 15 (2020) 67-73.
[14] A. Aslam, A.U. Rehman, N. Amin, M. Amami, M. Nabi, H. Alrobei, M. Asghar, N. Morley, M. Akhtar, M.I. Arshad, Sol-Gel auto-combustion preparation of M2+ = Mg2+, Mn2+, Cd2+ substituted M0.25Ni0.15Cu0.25Co0.35Fe2O4 ferrites and their characterizations, Journal of Superconductivity and Novel Magnetism, 35 (2022) 473-483.
https://doi.org/10.1007/s10948-021-06085-5
[15] N. Amin, A. Razaq, A.U. Rehman, K. Hussain, M. Nabi, N. Morley, M. Amami, A. Bibi, M.I. Arshad, K. Mahmood, Transport Properties of Ce-Doped Cd Ferrites CdFe2−xCexO4, Journal of Superconductivity and Novel Magnetism, (2021) 1-11.
https://doi.org/10.1007/s10948-021-06053-z
[16] M.I.U. Haq, M. Asghar, M.A.U. Nabi, N. Amin, S. Tahir, M.I. Arshad, Influence of Ce3+ and La3+ Substitution on Structural & Optical Parameters and Electrical Behavior on Mg-Zn Ferrites Synthesized via Co-precipitation method, Journal of Superconductivity and Novel Magnetism, 35 (2022) 719-732.
https://doi.org/10.1007/s10948-021-06124-1
[17] M.I. Arshad, M. Hasan, A.U. Rehman, M. Akhtar, N. Amin, K. Mahmood, A. Ali, T. Trakoolwilaiwan, N.T.K. Thanh, Structural, optical, electrical, dielectric, molecular vibrational and magnetic properties of La3+ doped Mg-Cd-Cu ferrites prepared by Co-precipitation technique, Ceramics International, 48 (2022) 14246-14260.
https://doi.org/10.1016/j.ceramint.2022.01.313
[18] G. Hussain, I. Ahmed, A.U. Rehman, M.U. Subhani, N. Morley, M. Akhtar, M.I. Arshad, H. Anwar, Study of the role of dysprosium substitution in tuning structural, optical, electrical, dielectric, ferroelectric, and magnetic properties of bismuth ferrite multiferroic, Journal of Alloys and Compounds, (2022) 165743.
https://doi.org/10.1016/j.jallcom.2022.165743
[19] G. Abbas, A.U. Rehman, W. Gull, M. Afzaal, N. Amin, L. Ben Farhat, M. Amami, N.A. Morley, M. Akhtar, M.I. Arshad, Impact of Co2+ on the spectral, optoelectrical, and dielectric properties of Mg0.25Ni0.25Cu0.5−xCoxFe1.97La0.03O4 ferrites prepared via sol-gel auto-combustion route, Journal of Sol-Gel Science and Technology, (2022) 1-15.
https://doi.org/10.1007/s10971-021-05713-9
[20] A. Nikolic, M. Boskovic, V. Spasojevic, B. Jancar, B. Antic, Magnetite/Mn-ferrite nanocomposite with improved magnetic properties, Materials Letters, 120 (2014) 86-89.
https://doi.org/10.1016/j.matlet.2014.01.023
[21] M.N. Akhtar, H.A. Siddiqa, M.S. Nazir, M.A. Khan, Preparations and tailoring of structural, magnetic properties of rare earths (REs) doped nanoferrites for microwave high frequency applications, Ceramics International, 46 (2020) 26521-26529.
https://doi.org/10.1016/j.ceramint.2020.07.118
[22] A.U. Rehman, N. Amin, M.B. Tahir, M.A. un Nabi, N. Morley, M. Alzaid, M. Amami, M. Akhtar, M.I. Arshad, Evaluation of spectral, optoelectrical, dielectric, magnetic, and morphological properties of RE3+ (La3+, and Ce3+) and Co2+ co-doped Zn0.75Cu0.25Fe2O4 ferrites, Materials Chemistry and Physics, 275 (2022) 125301.
https://doi.org/10.1016/j.matchemphys.2021.125301